TENMAK BOREN

BOR DERGİSİ
JOURNAL OF BORON
https://dergipark.org.tr/boron

Optimization for growth condition of ultrathin hexagonal boron nitride on dielectric substrates via LPCVD method

Meryem Bozkaya [1,*], **Muhammet Nasuh Arık** [2,3], **Ali Altuntepe** [4], **Hakan Ateş** [5], **Recep Zan** [6]

[1] *Gazi University, Graduate School of Natural and Applied Science, Advanced Technologies, Ankara, 06560, Türkiye*
[2] *Turkish Energy, Nuclear and Mineral Research Agency (TENMAK) Boron Research Institute, Ankara, 06510, Türkiye*
[3] *Ankara Yıldırım Beyazıt University, Faculty of Engineering and Natural Sciences, Metallurgical and Materials Engineering Ankara, 06800, Türkiye*
[4] *Sivas University of Science and Technology, Optical Excellence Application and Research Center, Sivas, 58000, Türkiye*
[5] *Gazi University, Faculty of Technology, Metallurgical and Materials Engineering, Ankara, 06560, Türkiye*
[6] *Niğde Ömer Halisdemir University, Faculty of Science, Physics Department, Niğde, 51240 Türkiye*

ARTICLE INFO

Article history:
Received December 15, 2025
Accepted January 23, 2026
Available online March 31, 2026

Research Article

DOI: 10.30728/boron.1840796

Keywords:
Deep ultraviolet photodetectors
Dielectric substrates
h-BN thin film
LPCVD
Non-catalytic effect

ABSTRACT

In this study, the direct and transfer-free synthesis of ultrathin hexagonal Boron Nitride (h-BN) films on non-catalytic quartz substrates was investigated using the Low-Pressure Chemical Vapor Deposition (LPCVD) method. The effects of key growth parameters, including growth duration (15-90 min), precursor amount (50-200 mg), and precursor decomposition temperature (80-100°C), were systematically investigated to achieve high-quality film growth. Spectroscopic characterization confirmed the formation of the h-BN phase, with Raman spectra exhibiting the characteristic E_{2g} vibrational mode and FT-IR analysis showing the distinct B-N stretching and B-N-B bending bonds at 1370 and 800 cm^{-1}, respectively. UV-Vis spectroscopy revealed high optical transparency (>95%) in the visible region, and Tauc plot analysis yielded an optical bandgap of 5.68 eV. This widening of the bandgap relative to bulk h-BN (~5.2 eV) provides quantitative evidence of the few-layer nature of the films due to the quantum confinement effect. The results demonstrate that the optimized LPCVD process allows for the precise control of h-BN synthesis on dielectric surfaces, eliminating the need for metal catalysts and complex transfer processes for optoelectronic applications.

1. Introduction

The development of optoelectronic devices operating in the deep ultraviolet (DUV) region [1] (~200-280 nm) is a crucial technological frontier with significant applications ranging from military surveillance and missile warning systems (MWS) to flame detection [2], non-line-of-sight (NLOS) optical communications [3], and biological agent sensing [4]. Devices targeting this range-known as the "solar-blind" region-offer a superior signal-to-noise ratio since natural solar radiation at these wavelengths is efficiently absorbed by the Earth's atmosphere's ozone layer [5]. Conventional wide bandgap semiconductors like gallium nitride (GaN) [6], silicon carbide (SiC) [7], and gallium oxide (Ga_2O_3) [8] have long been the primary materials for DUV photodetector fabrication [6-8]. However, the emergence of two-dimensional (2D) materials offers opportunities to address limitations such as high defect density, high processing costs, and the complexity associated with conventional bulk semiconductor fabrication [8, 9]. Among the 2D materials, hexagonal boron nitride (h-BN) stands out as an exceptional candidate for next-generation DUV applications [9, 10]. h-BN is a structural analog of graphene, possessing an ultra-wide bandgap (UWBG) typically around 6.0-6.4 eV [11], which naturally positions it to operate precisely within the DUV spectral window [12, 13]. Furthermore, h-BN exhibits outstanding physical and chemical properties, including superior mechanical strength, high thermal stability and conductivity, and a high absorption coefficient at the band edge ($7,5x10^5$ cm^{-1}) [14]. These combined attributes make h-BN highly desirable for creating robust, highly sensitive, and thermally stable photodetectors [15, 16]. For large-scale and high-quality synthesis, the Chemical Vapor Deposition (CVD) method remains the most scalable and controllable technique for h-BN [17]. However, traditional CVD processes necessitate the use of catalytic metal substrates, such as Cu [18] or Ni [19], to facilitate the growth. This approach inevitably introduces a critical technological hurdle: the resulting h-BN film must be transferred from the metallic catalyst onto the final target substrate (e.g., SiO_2 or quartz) for device integration [20, 21].

The transfer process is highly detrimental to the material's integrity [21]. It often leads to the incorporation

*Corresponding author: meryemm.bozkaya@gmail.com

of significant defects, including tears, folds, cracks, and chemical residues from the wet etching or polymer-assisted removal steps [21, 22]. These structural and chemical contaminations dramatically impair the material's crystalline quality and electronic properties, resulting in low reproducibility and compromised device performance-a major barrier to the commercialization of h-BN-based optoelectronics [23]. To circumvent the inherent drawbacks of the transfer process, the scientific community has been actively pursuing the direct synthesis of h-BN thin films onto dielectric or optically transparent substrates (Si, SiO_2, sapphire, quartz) where devices can be fabricated directly [23-26]. Despite the significant advantages, direct synthesis is challenging. The absence of a strong catalytic effect makes it difficult to achieve large-area uniformity, high crystallinity, and precise control over the film thickness, particularly in the ultra-thin regime necessary for high-performance 2D devices [27, 28].

This study addresses this critical challenge by focusing on the parameter optimization of the Low-Pressure Chemical Vapor Deposition (LPCVD) method for the direct synthesis of ultrathin h-BN films on non-catalytic quartz substrates. Quartz was selected due to its high thermal stability and excellent transparency in the ultraviolet region, which is essential for DUV photodetector applications. The primary objective of this work is to systematically investigate the correlation between key LPCVD growth parameters-specifically growth temperature, duration, and precursor concentration-and the resulting structural and optical quality of the h-BN films. The growth temperature was strategically limited to 1050°C to maintain the structural integrity of the quartz substrates while providing sufficient energy for the decomposition of ammonia borane (AB). This paper is organized as follows: Section 2 details the experimental methodology and the LPCVD setup. Section 3 presents the comprehensive characterization results and discusses the effects of the optimized parameters. Finally, Section 4 provides the main conclusions of the study. Through this systematic approach, the optimal synthesis conditions were determined to be 1050°C for 60 min with 150 mg of precursor decomposed at 80°C, providing a scalable and transfer-free pathway for high-performance h-BN-based optoelectronics.

2. Materials and Methods

2.1. Materials

The materials used for the synthesis and characterization of h-BN films were carefully selected and sourced. AB (97%, Boron Research Institute, Turkish Energy, Nuclear and Mineral Research Agency, Türkiye) is used as the precursor for boron and nitrogen. An ultrasonic bath (Bandelin, Germany) is used for cleaning the substrates. Additionally, the quartz substrates (1x1.5 cm^2, Süber Cam, Türkiye), a split furnace (Protherm Furnaces, Türkiye) and a vacuum pump (Value, China) were used for film growth.

2.2. Methods

The CVD method is widely used for the synthesis of ultra-thin h-BN films due to its environmentally friendly nature, suitability for large-scale production, tunability, and relatively low cost [17]. The setup used for the LPCVD system is shown schematically in Figure 1.

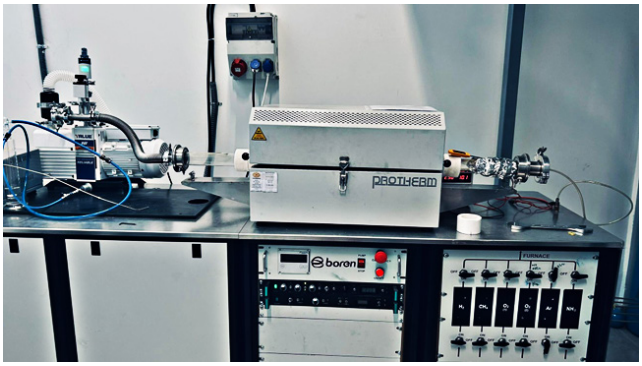

Figure 1. LPCVD system used for the h-BN growth.

First, 1×1.5 cm^2 quartz substrates were cleaned in an ultrasonic bath sequentially with acetone, isopropyl alcohol (IPA), and deionized water (DIW) for 15 minutes each. The cleaned substrates were dried with compressed air and swiftly loaded into a 120 cm long quartz tube with a 20 mm inner diameter. Subsequently, the AB precursor, contained in an alumina boat, was placed 50 cm away from the substrates, outside the main furnace, and heated using a heating belt. Prior to initiating the furnace, the system was subjected to two cycles of Ar purging to ensure the removal of residual oxygen. The furnace was then ramped up to the growth temperature at a rate of 10°C/min under a flow of 300 sccm of 10% Ar/H_2 (Argohid).

The selection of the growth temperature range (1000-1050°C) was based on literature indicating that high temperatures provide the necessary activation energy for the decomposition and nucleation of h-BN on non-catalytic surfaces. While temperatures up to 1100°C were initially considered, no stable film formation was observed at this level, likely due to the proximity to the softening point of the quartz substrate and potential desorption effects. Consequently, the optimization was focused between 1000°C and 1050°C [20, 23, 41]. The ranges for growth duration (15-90 min) and precursor amount (50-200 mg) were determined following an extensive literature review of transfer-free LPCVD processes to identify the thresholds for continuous film growth [21, 23].

As soon as the furnace reached the target temperature, the decomposition of the AB precursor was initiated via the heating belt. The system pressure prior to AB precursor decomposition was 6.5×10^{-2} mbar. A corresponding increase in partial pressure occurred during decomposition, depending on the amount of AB used. The specific synthesis parameters investigated

in this study are summarized in Table 1. Following the growth, the system was allowed to cool under a continuous flow of 500 sccm of 10% Ar/H_2 gas.

Table 1. Recipe of h-BN thin film synthesis.

Temperature	1000-1050ºC
Heating rate	10ºC/min.
Substrate used	Quartz
Type of carrier gas	%10 H_2 Argohid
Amount of carrier gas	300 sccm (270 sccm Ar; 30 sccm H_2)
Type and quantity of precursors	Ammonia Borane 50-200 mg
Precursor decomposition temperature	80-100 ºC
Pressure	6.5x10^{-1} mbar
Growth time	15-90 min.

3. Results and Discussion

To evaluate the success of the direct synthesis process, the structural, morphological, and optical properties of the h-BN films were first characterized using Raman spectroscopy (Renishaw, Wotton-under-Edge, UK), optical microscopy (Renishaw, Wotton-under-Edge, UK), and UV-Vis spectroscopy (UV-2700i Plus, Shimadzu, Kyoto, Japan). Raman spectroscopy was employed to confirm the structural quality and sp^2 phase of the h-BN film grown at 1050°C. The spectrum (Figure 2a) exhibits a sharp, intense characteristic peak at 1371 cm^{-1}, which is the definitive signature of the in-plane E2g phonon mode, validating the formation of the layered sp^2-bonded h-BN lattice [39]. However, secondary features were also observed, including a peak at 1031 cm^{-1} attributed to B-O stretching vibrations, reflecting minor oxygen incorporation or residual B_2O_3 byproducts [40]. This structural characterization is complemented by the optical microscopy image (Figure 2b), which confirms the film's excellent, near-complete coverage and highly uniform surface morphology across the large area of the quartz substrate. The successful formation of a large-area, morphologically uniform film without visible cracking on a dielectric substrate confirms the efficacy of the optimized LPCVD process.

The electronic structure of the synthesized h-BN films was further investigated using UV-Vis spectroscopy (Figure 3). The optical bandgap (E_g) was determined to be 5.68 eV through Tauc plot analysis (Figure 3inset). This value represents a significant blue-shift compared to the typical bandgap of bulk hexagonal boron nitride (5.2-5.4 eV). This widening of the bandgap is a direct consequence of the quantum confinement effect, which occurs as the film thickness is reduced to the few-layer regime [11, 13]. This quantitative finding, combined with the high optical transparency, provides solid evidence for the successful growth of ultrathin, few-layer h-BN films on non-catalytic quartz substrates.

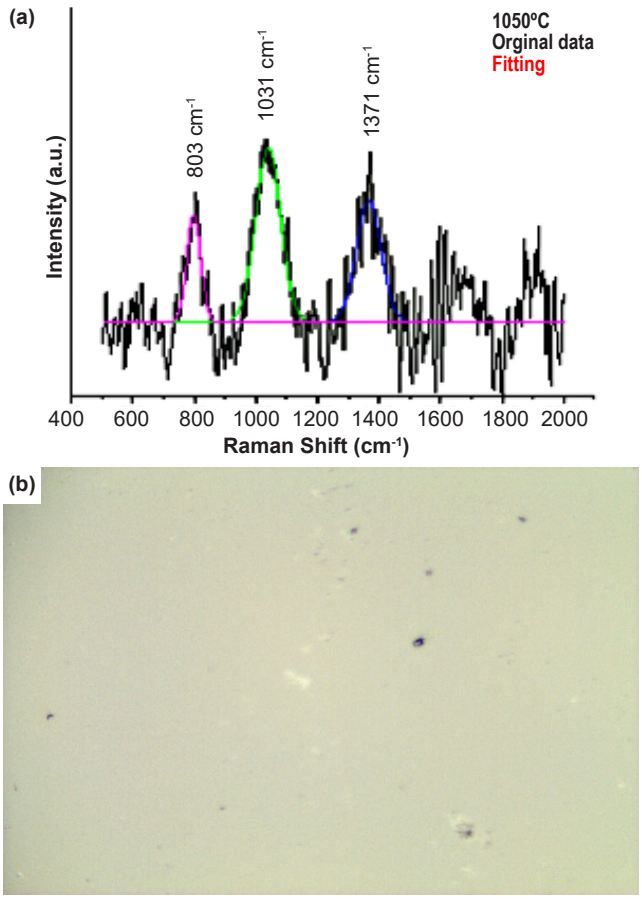

Figure 2. a) Raman Spectra of grown h-BN thin film b) Optic microscopy image of grown h-BN thin film on quartz substrate.

The chemical composition and bonding state of the h-BN films as a function of growth time were systematically investigated using X-ray Photoelectron Spectroscopy (XPS, K-Alpha, Thermo Fisher Scientific, US) and Fourier Transform Infrared Spectroscopy (FT-IR, Varian 660-IR, USA). The B1s and N1s core-level spectra consistently confirm the synthesis of the h-BN phase, with dominant peaks centered at approximately 191.02 eV and 398.52 eV, respectively. These values are characteristic of sp^2-bonded boron and nitrogen atoms [29]. Quantitative analysis of the optimal 60 min

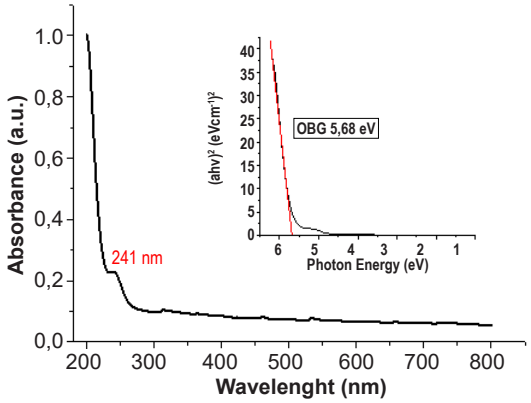

Figure 3. UV-Cis absorption spectra and (inset) optical band gap analysis.

film (Table 2) revealed a near-ideal B:N ratio of 1.02, while the narrow Full Width at Half Maximum (FWHM) values further validated a highly uniform bonding environment.

Table 2. XPS peak reasults of grown sample at 60 min.

Name	Start BE	Peak BE	End BE	FWHM eV	Atomic %
Si2p	109.98	107.03	103.28	2.4	11.47
C1s	290.58	285	281.88	2.54	11.21
B1s	199.98	191.02	187.78	2.98	16.62
N1s	403.08	398.52	394.88	2.28	16.27
O1s	537.48	532.91	528.88	2.29	22.21

Crucially, both XPS and FT-IR data demonstrate a synchronized evolution with increasing growth duration. As the deposition time extends from 15 min to 90 min, the intensity of the B1s and N1s XPS peaks increases significantly. This observation is corroborated by the FT-IR spectra, where the characteristic absorption bands at 1373 cm^{-1} (in-plane B-N stretching) and 784 cm^{-1} (out-of-plane B-N-B bending) exhibit a visible enhancement in signal strength (Figure 4). Given that the synthesis occurs on an inert quartz substrate via a non-catalytic mechanism, this consistent trend across both spectroscopic techniques provides direct evidence that the film thickness is precisely controllable by the deposition time.

Furthermore, the Si2p XPS core-level spectra show a notable attenuation in intensity as growth time increases, while the FT-IR spectra display a dominant Si-O-Si stretching band around 1000-1100 cm^{-1} originating from the substrate [14, 15]. The attenuation of the Si2p signal alongside the strengthening of h-BN vibrational modes confirms that the growing h-BN film acts as an effective overlayer, gradually covering the dielectric surface. The absence of significant shifts in the h-BN peak positions between 15 and 60 minutes suggests that the chemical environment and sp^2 hybridization remain stable throughout the growth process, supporting the high structural integrity of the optimized ultrathin films.

Regarding the presence of oxygen in the chemical analysis, the high O1s atomic percentage (22.21%) observed in the XPS data is primarily attributed to the underlying quartz (SiO_2) substrate rather than intrinsic film contamination. This is corroborated by the simultaneous detection of a significant Si2p signal (11.47%) and the broad Si-O-Si stretching bands observed in the FT-IR spectra between 1000 and 1100 cm^{-1}. Given that the XPS sampling depth exceeds the thickness of the ultrathin h-BN overlayer, the photoelectrons from the substrate contribute substantially to the total signal. However, a minor contribution from surface-adsorbed oxygen or hydroxyl groups due to ambient exposure cannot be entirely ruled out. The absence of a distinct B-O vibration in the FT-IR spectra and the symmetric nature of the B1s and N1s peaks further suggest that the h-BN lattice itself remains largely free of significant oxidation, maintaining its structural integrity on the dielectric surface [30].

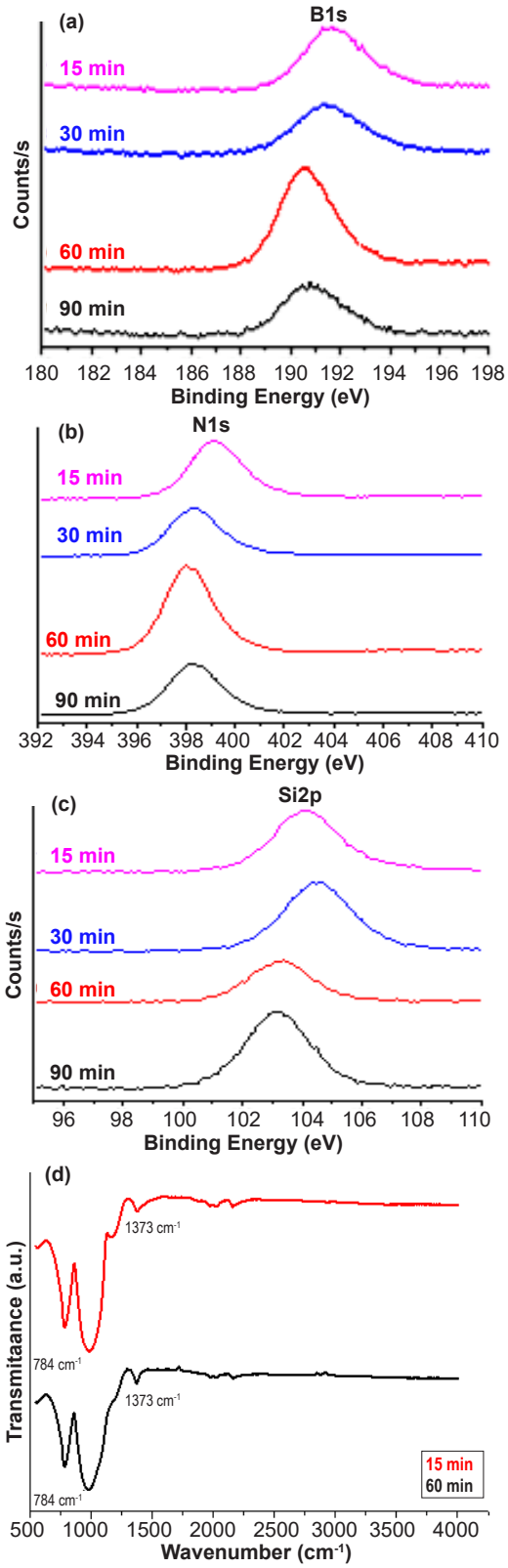

Figure 4. XPS analysis of samples grown at 1050°C for 90-60-30-15 min. a) B1s b)N1s c) Si2p d) FT-IR spectra of grown sample at different AB precursor amount 60 min and 15 min.

The influence of the AB precursor mass on the synthesized h-BN films was investigated while keeping the growth temperature and duration constant at 1050°C and 60 minutes. The B1s and N1s core-level spectra (Figures 5a and 5b) consistently demonstrate that the characteristic sp^2 bonding energy remains stable, indicating that the AB amount does not alter the chemical phase of the product.

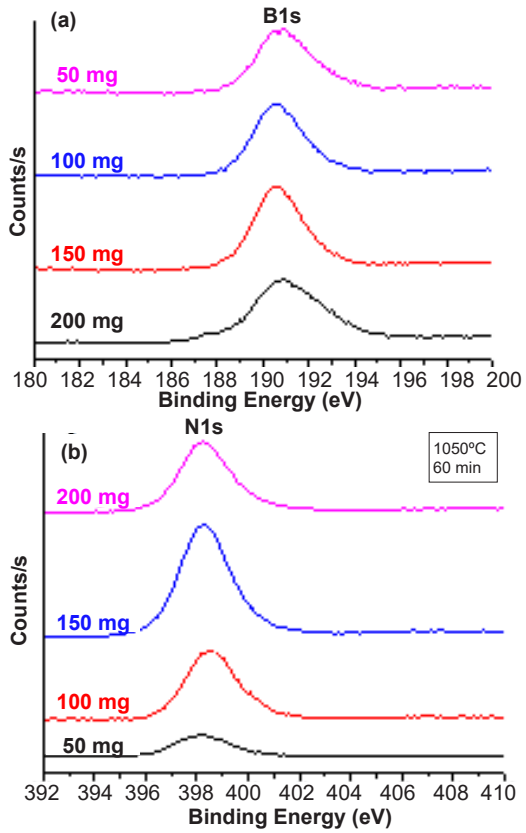

Figure 5. XPS analysis of samples grown at 1050°C for 200-150-100-50 mg AB precursor a) B1s b) N1s.

Quantitative analysis of the optimized 150 mg film (Table 3) confirmed high chemical purity and ideal stoichiometry, with a resulting B:N ratio of 1.03. The narrow FWHM values (2.49 eV for B1s and 2.27 eV for N1s) are highly desirable for high-quality h-BN films and demonstrate that the 150 mg mass provides sufficient precursor without promoting excessive boron-rich defects.

Table 3. XPS peak reasults of grown sample with 150 mg AB.

Name	Start BE (eV)	Peak BE (eV)	End BE (eV)	FWHM (eV)	Atomic Ratio (%)
Si2p	107.18	103.17	98.78	2.36	11.3
C1s	195.48	190.58	185.88	2.49	32.36
B1s	290.78	284.75	280.58	2.66	8.94
N1s	402.88	398.26	394.08	2.27	31.37
O1s	537.98	532.67	528.18	2.23	16.03

A significant observation is the proportional increase in the intensity of both the B1s and N1s signals as the precursor mass is increased from 50 mg to 150 mg. This relationship confirms that the h-BN synthesis operates under a precursor-limited kinetic regime [21]. In this regime, increasing the solid AB mass leads to a higher concentration of active boron and nitrogen species in the gas phase, directly translating to a higher growth rate and a thicker h-BN film yield within the fixed growth duration.

However, further investigation via FT-IR spectroscopy revealed a critical threshold for structural purity. While the characteristic h-BN peaks remained dominant for the 150 mg sample, the FT-IR spectrum of the 200 mg sample exhibited an additional shoulder near 1132 cm^{-1} (Figure 6). This peak is attributed to C-B stretching or the formation of amorphous boron phases, indicating that excessive precursor amounts initiate the incorporation of undesirable bond configurations. Consequently, 150 mg was established as the optimal precursor mass for achieving precise control over thickness while maintaining the high-purity sp^2 hybridization required for high-performance h-BN-based optoelectronics.

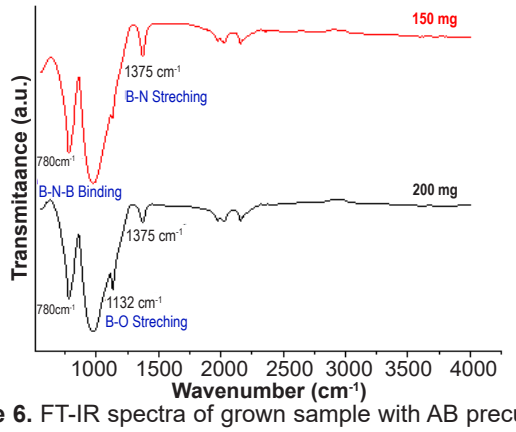

Figure 6. FT-IR spectra of grown sample with AB precursor amounts 200 and 150 mg.

Finally, the ultrathin nature of the films produced under these optimized conditions was quantitatively confirmed by the optical bandgap (E_g) of 5.68 eV obtained from Tauc plot analysis. This significant blue-shift relative to the bulk h-BN value (~5.2 eV) is a direct consequence of the quantum confinement effect, providing conclusive evidence that the optimized LPCVD process yields high-quality, few-layer h-BN structures directly on dielectric quartz substrates.

The influence of the AB precursor decomposition temperature (T_{dec}) on the resulting h-BN film was investigated while fixing the synthesis temperature and duration at 1050°C for 60 min. The B1s and N1s core-level spectra (Figures 7a and 7b) consistently show that the sp^2 bonding energy remains unchanged, validating that the chemical phase of the product is stable h-BN. Quantitative analysis of the film synthesized at the optimal 80°C T_{dec} confirmed outstanding stoichiometry and chemical homogeneity (Table 4). The B1s and N1s atomic percentages, recorded at 33.83% and

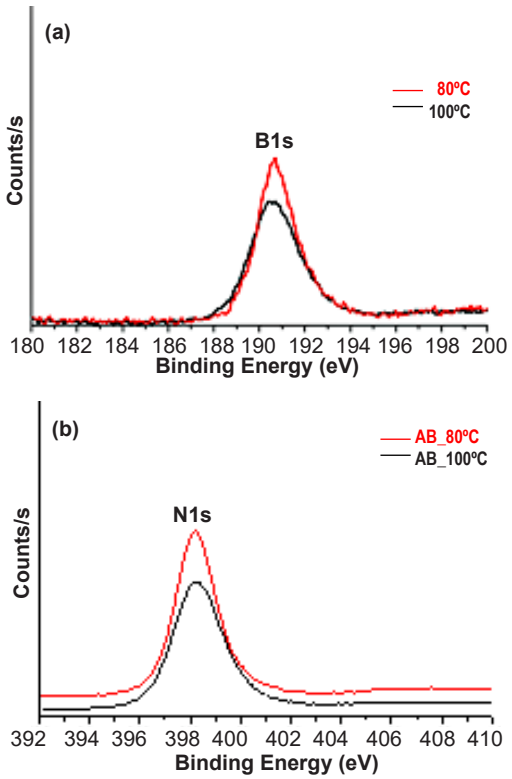

Figure 7. XPS analysis of samples grown at 1050°C for 100°C and 80°C AB decomposition temperature a) B1s b) N1s.

33.34% respectively, yielded a near-perfect B:N ratio of 1.01, affirming high film purity. Furthermore, the exceptionally narrow and identical FWHM values for both B1s and N1s peaks (1.88 eV) demonstrate a highly uniform bonding environment, suggesting superior crystalline quality under these controlled thermal conditions.

A notable difference is observed in the peak intensities, where the film synthesized with a T_{dec} of 80°C exhibits a higher signal intensity compared to the film grown at 100°C. The precursor decomposition temperature is a critical factor that controls the flux of active B-N species delivered to the reactor. In the non-catalytic LPCVD growth regime, the lower decomposition temperature of 80°C facilitates a slower, more controlled, and sustained release of the precursor. This controlled flux promotes more efficient surface adsorption and lateral growth, resulting in a more uniform h-BN film coverage than the rapid and potentially inefficient delivery achieved at 100°C.

Table 4. XPS peak reasults of grown sample at 80°C.

Name	Start BE (eV)	Peak BE (eV)	End BE (eV)	FWHM (eV)	Atomic % (eV)
Si2p	107.38	103.43	99.48	2.18	8.89
C1s	195.58	190.65	186.28	1.88	33.83
B1s	291.68	284.89	280.98	2.13	10.16
N1s	403.18	398.19	394.08	1.88	33.34
O1s	538.08	532.67	527.78	2.1	13.77

Consistent with the previously discussed oxygen analysis, the observed O1s (13.77%) and Si2p (8.89%) signals at this optimized T_{dec} further confirm that the h-BN film is in the ultrathin regime, allowing the XPS signals from the underlying SiO_2 substrate to be detected. The high quality of the sp^2 lattice at 80°C T_{dec}, combined with the earlier confirmed optical bandgap of 5.68 eV, demonstrates that managing the precursor flux is essential for maintaining the quantum confinement effect while achieving high-quality crystal growth on dielectric surfaces.

The optical quality and presence of deep-level defects in the h-BN films synthesized at 1000°C and 1050°C were investigated using photoluminescence spectroscopy (PL, FS5 Spectrofluorometer, Edinburgh Instruments,UK). Both spectra (Figure 8) display prominent, broad-band emission peaks in the visible region, specifically centered around 480 nm, 570 nm, and 610 nm. These features are highly characteristic of deep-level defect emissions frequently observed in h-BN materials grown via CVD. While the intrinsic bandgap emission of bulk h-BN is in the deep ultraviolet region, these visible emissions are generally attributed to structural defects such as boron vacancies (V_B), nitrogen vacancies (V_N), or oxygen-related complexes, which form radiative defect states within the bandgap.

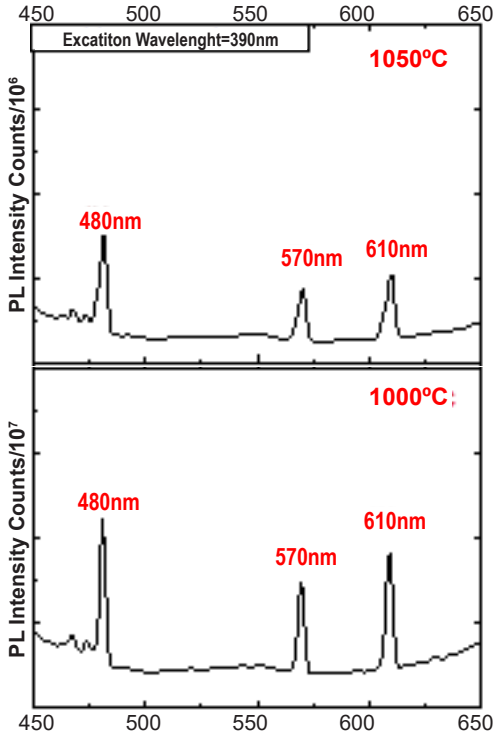

Figure 8. PL spectra of grown samples at 1050°C and 1000°C.

This optical behavior is further elucidated by the FT-IR analysis (Figure 9), which provides a direct comparison of the structural evolution at different temperatures. For the film grown at 1050°C, the characteristic absorption bands at 1373 cm^{-1} (in-plane B-N stretching) and 786 cm^{-1} (out-of-plane B-N-B bending) are significantly more

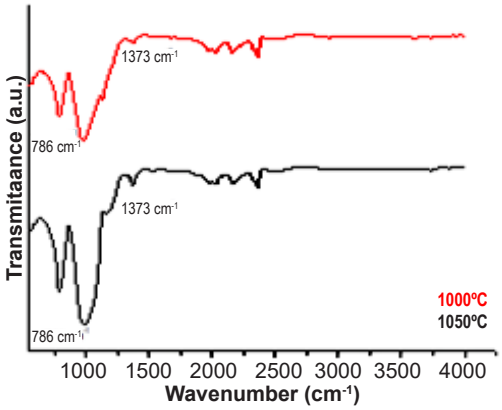

Figure 9. FT-IR spectra of grown sample at 1000°C and 1050°C.

intense and well-defined compared to those grown at 1000°C. The enhancement in these vibrational modes indicates that the higher growth temperature facilitates better nucleation and a higher deposition rate on the non-catalytic quartz surface, leading to improved structural order and increased film thickness.

Comparing the two synthesis temperatures, the film grown at 1050°C exhibits a higher overall PL intensity across all observed defect peaks. This enhancement is consistent with the FT-IR results, suggesting that the higher temperature results in a higher volume of emitting material (thicker film) and potentially a higher concentration of the specific radiative defects associated with improved crystalline domains. Given that the synthesis goal is to maximize film yield on dielectric substrates, the correlated enhancement in both PL and FT-IR signals confirms that 1050°C is the more effective temperature for establishing the desired h-BN structure and thickness.

The comparative quantitative XPS analysis across the three optimized parameter conditions reveals a critical kinetic effect on film growth, thickness, and purity. While all films maintained excellent stoichiometry (B: N ratios between 1.01 and 1.03), the total h-BN signal varied dramatically, with the 80°C T_{dec} and 150 mg AB films showing nearly double the combined B and N signal (approximately 67.17% and 63.73%, respectively) compared to the 60 min growth time sample (approximately 32.89%).

This significant increase in the h-BN signal confirms that the 80°C T_{dec} and 150 mg AB parameters effectively break the bottleneck of the non-catalytic growth regime. The kinetic advantage is fully demonstrated by the substrate signal attenuation: the 80°C T_{dec} film minimizes the Si2p signal from the underlying quartz to its lowest level (8.89%), validating that this condition yields the highest film thickness and most complete coverage.

Furthermore, this optimal kinetic control simultaneously resulted in the highest film quality: the 80°C T_{dec} sample registered the lowest O impurity signal (13.77% O1s atomic percentage) and the narrowest FWHM (1.88 eV) for both B1s and N1s peaks. This suggests that the slow, controlled precursor flux at 80°C not only maximizes the growth rate but also minimizes the incorporation of oxygen-related defects (as corroborated by the FT-IR analysis), yielding the most uniform and chemically pure h-BN film across all tested parameters.

4. Conclusions

This study successfully demonstrated the direct synthesis of high-quality, few-layer h-BN thin films on non-catalytic quartz substrates via the LPCVD method, effectively eliminating the need for the defect-inducing transfer processes. Comprehensive spectroscopic analyses confirmed the formation of the desired sp^2-bonded h-BN phase, validated by the characteristic E_{2g} Raman mode (1371 cm^{-1}), h-BN vibrational modes in FT-IR (1373 cm^{-1} and 784 cm^{-1}), and consistent B1s/N1s XPS binding energies.

The growth kinetics were established to be precursor-limited, allowing for precise control over film thickness through growth duration and precursor mass. A significant finding was the blue-shift of the optical bandgap to 5.68 eV, as determined by Tauc plot analysis. This widening, compared to the bulk h-BN value, provides conclusive evidence of the quantum confinement effect, confirming the ultrathin nature of the synthesized films. Optimization of the thermal parameters showed that a growth temperature of 1050°C and a precursor decomposition temperature of 80°C provided the ideal activation energy and controlled flux for maximizing film yield and crystalline quality. While FT-IR and Raman analyses identified minor oxygen-related signals, XPS depth-sensitive data confirmed these originated primarily from the underlying SiO_2 substrate, rather than intrinsic film contamination.

Morphological characterization revealed excellent large-area coverage and high uniformity, confirming the efficacy of the direct growth strategy. By successfully determining the optimal conditions-1050°C for 60 min with 150 mg of precursor-this work establishes a robust, scalable, and contamination-free pathway for producing high-performance h-BN films, paving the way for advanced DUV optoelectronic applications.

5. Acknowledgements

This work was supported by The Scientific and Technological Research Council of Türkiye (TÜBİTAK) under the 1002-A Short-Term Support Module (Project No: 225M094).

6. Author Contribution Statement

Meryem Bozkaya: Conceptualization, methodology, execution of the (LPCVD) synthesis, primary investigation, data collection, writing-original draft preparation and formal analysis of all characterization

data.

Muhammet Nasuh Arık: Formal analysis (specifically the XPS data interpretation), writing-review and editing.

Ali Altuntepe: Characterization and experimental investigation.

Hakan Ateş: Supervision, writing-review and editing.

Recep Zan: Supervision, writing-review and editing.

7. Conflict of Interest

No conflict of interest was declared by the authors.

References

[1] Liu, X., Lv, Z., Liao, Z., Sun, Y., Zhang, Z., Sun, K., ... & Zhou, S. (2024). Highly efficient AlGaN-based deep-ultraviolet light-emitting diodes: from bandgap engineering to device craft. *Microsystems & Nanoengineering*, *10*(1), 110. https://doi.org/10.1038/s41378-024-00737-x

[2] Long, J. P., Varadaraajan, S., Matthews, J., & Schetzina, J. F. (2002). UV detectors and focal plane array imagers based on AlGaN pin photodiodes. *Optoelectronics Review*, (4), 251-260.

[3] Cao, T., Wang, P., Wu, T., Wang, M., Zhang, H., Wang, K., & Song, J. (2025). Performance analysis of non-line-of-sight ultraviolet communications under periodic pulse jamming attack through turbulent channels. *Optics Express*, *33*(17), 35146-35163. https://doi.org/10.1364/OE.566788

[4] Sharma, V. K., & Demir, H. V. (2022). Bright future of deep-ultraviolet photonics: Emerging UVC chip-scale light-source technology platforms, benchmarking, challenges, and outlook for UV disinfection. *ACS Photonics*, *9*(5), 1513-1521. https://doi.org/10.1021/acsphotonics.2c00041

[5] Hao, J., Li, L., Gao, P., Jiang, X., Ban, C., & Shi, N. (2023). Deep ultraviolet detectors based on wide bandgap semiconductors: a review. *Journal of Nanoparticle Research*, *25*(4), 81. https://doi.org/10.1007/s11051-023-05694-6

[6] Chen, R., Li, Q., Zhang, Q., Li, J., Zhang, Z., Fang, W., ... & Hao, Y. (2023). High-crystallinity and high-temperature S-stability of the hexagonal boron nitride film grown on sapphire. *Crystal Growth & Design*, *23*(12), 8783-8792. https://doi.org/10.1021/acs.cgd.3c00902

[7] Veeralingam, S., Durai, L., Yadav, P., and Badhulika, S. (2021). Record-high responsivity and detectivity of a flexible deep-ultraviolet photodetector based on solid state-assisted synthesized hBN nanosheets. *ACS Applied Electronic Materials*, *3*(3), 1162-1169. https://doi.org/10.1021/acsaelm.0c01021

[8] Kaushik, S., & Singh, R. (2021). 2D layered materials for ultraviolet photodetection: A review. *Advanced Optical Materials*, *9*(11), 2002214. https://doi.org/10.1002/adom.202002214

[9] Fang, W., Li, Q., Li, J., Li, Y., Zhang, Q., Chen, R., & Wang, T. (2023). Deep ultraviolet photodetector: Materials and devices. *Crystals*, *13*(6), 915. https://doi.org/10.3390/cryst13060915

[10] Lv, J., Lu, X., Li, X., Xu, M., Zhong, J., Zheng, X., … & Zhang, Q. (2022). Epitaxial growth of lead-free 2D Cs3Cu2I5 perovskites for high-performance UV photodetectors. *Small*, *18*(27), 2201715. https://doi.org/10.1002/smll.202201715

[11] Zhang, K., Feng, Y., Wang, F., Yang, Z., & Wang, J. (2017). Two-dimensional hexagonal boron nitride (2D-hBN): Synthesis, properties and applications. *Journal of Materials Chemistry C*, *5*(46), 11992-12022. https://doi.org/10.1039/C7TC04300G

[12] Zhang, J., Tan, B., Zhang, X., Gao, F., Hu, Y., Wang, L., … & Hu, P. (2021). Atomically thin hexagonal boron nitride and its heterostructures. *Advanced Materials*, *33*(6), 2000769. https://doi.org/10.1002/adma.202000769

[13] Lin, C. H., Fu, H. C., Cheng, B., Tsai, M. L., Luo, W., Zhou, L., ... & He, J. H. (2018). A flexible solar-blind 2D boron nitride nanopaper-based photodetector with high thermal resistance. *2D Materials and Applications*, *2*(1), 23. https://doi.org/10.1038/s41699-018-0070-6

[14] Li, J., Majety, S., Dahal, R., Zhao, W. P., Lin, J. Y., & Jiang, H. X. (2012). Dielectric strength, optical absorption, and deep ultraviolet detectors of hexagonal boron nitride epilayers. *Applied Physics Letters*, *101*(17). https://doi.org/10.1063/1.4764533

[15] Zhang, X., Yang, H., Su, Z., Tian, Y., Feng, Y., Ding, Y., … & Hu, P. (2025). Ultraflat single-crystal hexagonal boron nitride film grown on Cu/Ni (1 1 1) for high-performance deep ultraviolet photodetectors. *Chemical Engineering Journal*, 163316. https://doi.org/10.1016/j.cej.2025.163316

[16] Chen, X., Tan, C., Liu, X., Luan, K., Guan, Y., Liu, X., … & Chen, Z. (2021). Growth of hexagonal boron nitride films on silicon substrates by low-pressure chemical vapor deposition. *Journal of Materials Science: Materials in Electronics*, *32*, 3713-3719. https://doi.org/10.1007/s10854-020-05116-6

[17] Li, L., Chen, H., Fang, Z., Meng, X., Zuo, C., Lv, M., … & Ding, L. (2020). An electrically modulated single-color/dual-color imaging photodetector. *Advanced Materials*, *32*(24), 1907257. https://doi.org/10.1002/adma.201907257

[18] Sutter, P., Lahiri, J., Zahl, P., Wang, B., & Sutter, E. (2013). Scalable synthesis of uniform few-layer hexagonal boron nitride dielectric films. *Nano Letters*, *13*(1), 276-281. https://doi.org/10.1021/nl304080y

[19] Li, D., Gao, W., Sun, X., Yu, H., Liu, C., & Yin, H. (2021). Direct growth of hexagonal boron nitride thick films on dielectric substrates by ion beam assisted deposition for deep-UV photodetectors. *Advanced Optical Materials*, *9*(12), 2100342. https://doi.org/10.1002/adom.202100342

[20] Li, Q., Wu, Q., Gao, J., Wei, T., Sun, J., Hong, H., … & Liu, Z. (2018). Direct growth of 5 in. uniform hexagonal boron nitride on glass for high-performance deep-ultraviolet light-emitting diodes. *Advanced Materials Interfaces*, *5*(18), 1800662. https://doi.org/10.1002/admi.201800662

[21] Behura, S., Nguyen, P., Debbarma, R., Che, S., Seacrist,

M. R., & Berry, V. (2017). Chemical interaction-guided, metal-free growth of large-area hexagonal boron nitride on silicon-based substrates. *ACS Nano*, *11*(5), 4985-4994. https://doi.org/10.1021/acsnano.7b01666

[22] Gao, M., Meng, J., Chen, Y., Ye, S., Wang, Y., Ding, C., & Zhang, X. (2019). Catalyst-free growth of two-dimensional hexagonal boron nitride few-layers on sapphire for deep ultraviolet photodetectors. *Journal of Materials Chemistry C*, *7*(47), 14999-15006. https://doi.org/10.1039/C9TC05206B

[23] Singhal, R., Echeverria, E., McIlroy, D. N., & Singh, R. N. (2021). Synthesis of hexagonal boron nitride films on silicon and sapphire substrates by low-pressure chemical vapor deposition. *Thin Solid Films*, *733*, 138812. https://doi.org/10.1016/j.tsf.2021.138812

[24] Li, D., Gao, W., Sun, X., Yu, H., Liu, C., & Yin, H. (2021). Direct growth of hexagonal boron nitride thick films on dielectric substrates by ion beam assisted deposition for deep-UV photodetectors. *Advanced Optical Materials*, *9*(12), 2100342. https://doi.org/10.1002/adom.202100342

[25] Chen, R., Li, Q., Zhang, Q., Li, J., Zhang, Z., Fang, W., … & Hao, Y. (2023). High-crystallinity and high-temperature stability of the hexagonal boron nitride film grown on sapphire. *Crystal Growth & Design*, *23*(12), 8783-8792. https://doi.org/10.1021/acs.cgd.3c00902

[26] Aldalbahi, A., & Feng, P. (2015). Development of 2-D boron nitride nanosheets UV photoconductive detectors. *IEEE Transactions on Electron Devices*, *62*(6), 1885-1890. https://doi.org/10.1109/TED.2015.2423253

[27] Roy, S., Zhang, X., Puthirath, A. B., Meiyazhagan, A., Bhattacharyya, S., Rahman, M. M., … & Ajayan, P. M. (2021). Structure, properties and applications of two dimensional hexagonal boron nitride. *Advanced Materials*, *33*(44), Article 2101589. https://doi.org/10.1002/adma.202101589

[28] Cao, F., Liu, Y., Liu, M., Han, Z., Xu, X., Fan, Q., & Sun, B. (2024). Wide bandgap semiconductors for ultraviolet photodetectors: Approaches, applications, and prospects. *Research*, *7*, 0385. https://doi.org/10.34133/research.0385

[29] Chalmpes, N., Bourlinos, A. B., Alsmaeil, A. W., Aljarrah, A. S., Salmas, C. E., Karakassides, M. A., & Giannelis, E. P. (2024). First synthesis of 2D materials by hypergolic reactions and evaluation of their dispersions for ink formulation: Hexagonal boron nitride and fluorinated carbon nanosheets. *Materials Research Express*, *11*(3), 035002. https://doi.org/10.1088/2053-1591/ad2d42

[30] Zemlyanov, D. Y., Jespersen, M., Zakharov, D. N., Hu, J., Paul, R., Kumar, A., ... & Voevodin, A. A. (2018). Versatile technique for assessing thickness of 2D layered materials by XPS. *Nanotechnology*, *29*(11), 115705. https://doi.org/10.1088/1361-6528/aaa6ef

[31] Weston, L., Wickramaratne, D., Mackoit, M., Alkauskas, A., & Van de Walle, C. G. (2018). Native point defects and impurities in hexagonal boron nitride. P*hysical Review B*, *97*(21), 214104. https://doi.org/10.1103/PhysRevB.97.214104

[32] Rousseau, A., Valvin, P., Elias, C., Xue, L., Li, J., Edgar, J. H., ... & Cassabois, G. (2022). Stacking-dependent deep level emission in boron nitride. *Physical Review Materials*, *6*(9), 094009. https://doi.org/10.1103/PhysRevMaterials.6.094009

[33] Chen, X., Yue, X., Zhang, L., Xu, X., Liu, F., Feng, M., ... & Fu, X. (2024). Activated single photon emitters and enhanced deep-level emissions in hexagonal boron nitride strain crystal. *Advanced Functional Materials*, *34*(1), 2306128. https://doi.org/10.1002/adfm.202306128

[34] Du, X. Z., Li, J., Lin, J. Y., & Jiang, H. X. (2015). The origin of deep-level impurity transitions in hexagonal boron nitride. *Applied Physics Letters*, *106*(2). https://doi.org/10.1063/1.4905908

[35] Tsushima, E., Tsujimura, T., & Uchino, T. (2018). Enhancement of the deep-level emission and its chemical origin in hexagonal boron nitride. *Applied Physics Letters*, *113*(3). https://doi.org/10.1063/1.5038168

[36] Choutipalli, V. S. K., Esackraj, K., Varathan, E., & Subramanian, V. (2022). Vacancy defect assisted enhanced nitrogen fixation in boron nitride nanomaterials. *Applied Surface Science*, *602*, 154406. https://doi.org/10.1016/j.apsusc.2022.154406

[37] Singh, B., Kaur, G., Singh, P., Singh, K., Kumar, B., Vij, A., ... & Kumar, A. (2016). Nanostructured boron nitride with high water dispersibility for boron neutron capture therapy. *Scientific Reports*, *6*(1), 35535. https://doi.org/10.1038/srep35535

[38] Shen, T., Liu, S., Yan, W., & Wang, J. (2019). Highly efficient preparation of hexagonal boron nitride by direct microwave heating for dye removal. *Journal of Materials Science*, *54*(12), 8852-8859. https://doi.org/10.1007/s10853-019-03514-8

[39] Huang, C., Chen, C., Ye, X., Ye, W., Hu, J., Xu, C., & Qiu, X. (2013). Stable colloidal boron nitride nanosheet dispersion and its potential application in catalysis. *Journal of Materials Chemistry A*, *1*(39), 12192-12197. https://doi.org/10.1039/C3TA12231J

[40] Stefanovsky, S. V., Fox, K. M., & Marra, J. C. (2013). Infrared and Raman spectroscopic study of glasses in the Al2O3-B2O3-Fe2O3-Na2O-SiO2 System. *MRS Online Proceedings Library (OPL)*, 1518, 53-58. https://doi.org/10.1557/opl.2013.143

[41] Xu, H., Li, K., Tan, Z., Jia, J., Wang, L., & Chen, S. (2025). Recent advances in chemical vapor deposition of hexagonal boron nitride on insulating substrates. *Nanomaterials*, *15*(14), 1059. https://doi.org/10.3390/nano15141059